

Crystallization kinetics of $\text{La}_2\text{O}_3\text{--Al}_2\text{O}_3\text{--B}_2\text{O}_3$ glass–ceramic composites

Chih-Lung Chen^a, Wen-Cheng J. Wei^{a,*}, Andreas Roosen^b

^a Institute of Materials Science & Engineering, National Taiwan University, 1 Roosevelt Road, Sect. 4, Taipei 106, Taiwan, ROC

^b Institute of Materials Science, Glass and Ceramics, University of Erlangen-Nuremberg, Erlangen, Germany

Received 11 April 2005; received in revised form 8 August 2005; accepted 14 August 2005

Available online 21 October 2005

Abstract

One glass formulation (L2 glass) with the composition of La_2O_3 , Al_2O_3 and B_2O_3 in a molar ratio of 10:10:80 was selected to cofire with Al_2O_3 filler. The composites underwent a two-stage crystalline evolution in the temperature range of 800 to 975 °C. The crystallization kinetics of LaBO_3 grains and the transformation to $\text{LaAl}_2\text{B}_3\text{O}_9$ phase were investigated by DTA, XRD, SEM/EDS, and TEM. The results showed that the Al_2O_3 filler plays an important role as the heterogeneous sites of LaBO_3 nuclei, and as reactant for the formation of flaky $\text{LaAl}_2\text{B}_3\text{O}_9$ crystals. The apparent activation energy of LaBO_3 -phase formation in L2 glass was 534 kJ/mol and reduced to 466 kJ/mol by the addition of Al_2O_3 . The detail transformation reactions, kinetics, and the crystalline orientation relationship between those phases are reported.

© 2005 Elsevier Ltd. All rights reserved.

Keywords: LAB glass; Composite; Microstructure; Transformation; Crystallization; Glass ceramics

1. Introduction

A low-firing temperature (<900 °C), lead-free, nonalkali, and low dielectric constant and low-dielectric loss system, $\text{La}_2\text{O}_3\text{--Al}_2\text{O}_3\text{--B}_2\text{O}_3$ (LAB) glass–ceramic materials have been synthesized and investigated.^{1,2} The composition was simplified from DuPont 943 tape system,³ and developed for the application of low-temperature cofiring ceramics (LTCC). The processing window of the LAB glass, determined by various thermal and wetting measurements, indicated that the initial shrinkage temperature of the glass could be as low as 700 °C. In particular, one glass composition (L2 glass) with a composition of La_2O_3 10 mol%, Al_2O_3 10 mol%, and B_2O_3 80 mol% was identified to have the most suitable sintering properties when doped with Al_2O_3 particles as a filler phase in a mass ratio of 30/70. The sintered composite has three major crystal phases, namely Al_2O_3 , LaBO_3 crystals, and flaky $\text{LaAl}_2\text{B}_3\text{O}_9$ crystal after sintering at 850 °C.²

In addition to sintering, the crystallization of glass–ceramics during heat treatments is also interesting. Several papers^{4,5} have reported the influence of seeding and reduction of the activation energy in γ - or θ - to α - Al_2O_3 transformation. The other cases,

e.g. ZrO_2 nanopowder⁶, were used as nucleating agents for $\text{CaO--P}_2\text{O}_5\text{--SiO}_2$ glass system, of which the activation energy of apatite/wollastonite/leucite phases could be decreased from 477 to 375 kJ/mol owing to the increase of nucleation sites. Beside the seeding effect, detail microstructural quantifications were conducted in order to investigate the crystallization mechanisms of nucleation and growth in many oxide systems.^{4–8}

The aims of previous investigations^{1,2} were to study the processing characteristics of LAB/ Al_2O_3 glass–ceramic composites and to evaluate its potential for LTCC application. The aims of this study were to quantify the microstructural characteristics and crystallization kinetics of two crystalline phases of the glass–ceramic composites, so as to understand the crystallization behavior in the temperature region between 800 and 950 °C.

2. Experimental procedure

2.1. Materials and sample preparation

Two precursor powders were used. One was a La–Al–B–O glass (L2) powder in a composition shown in Table 1 prepared by the steps specified in our previous work.^{1,2} The other was an Al_2O_3 powder (A32, Sumitomo Chemical Corp., Tokyo, Japan). The powder mixtures (e.g. L30A with 30 mass% Al_2O_3) were prepared by the following steps.

* Corresponding author. Fax: +886 2 2363 2684.
E-mail address: wjwei@ntu.edu.tw (W.-C.J. Wei).

Table 1
Composition of L2 glass and alumina powders

	L2 glass ^a	A32 ^b
La ₂ O ₃	10 (mol%)	–
Al ₂ O ₃	12	99.5+
Ba ₂ O ₃	78	–
SiO ₂	–	0.07
Fe ₂ O ₃	–	0.04
Na ₂ O	–	0.04
Phase	Amorphous	α-Phase
Mean particle size (μm)	1.56	1.04

^a Analyzed by ICP-OES.

^b Data given by manufacturer.

The powders were firstly dispersed in the mixture of methyl ethyl ketone (MEK) and ethanol. The slurry was ball-milled for 24 h, then dried in an oven at 70 °C overnight. The admixture was sieved through 140 mesh and granulation before die-pressing. The green disk in the diameter of 5.0 mm and a thickness of ca. 7 mm was prepared by die-pressing at 80 MPa.

The L2 glass and L30A specimens were sintered at 800 °C for 1 h, and/or heat-treated at 850–950 °C for 10–30 min. The heating rate was normally set at 10 °C/min. The composites was sintered in air and cooled in air furnace.

The determination of crystallization kinetic parameters of L30A glass–ceramic composite was performed by nonisothermal methods. The investigations of the DTA data with different heating rates were conducted using pulverized L2 glass and L30A glass–ceramic samples. Although two crystalline phases, equiaxial LaBO₃ and flaky LaAl₂B₃O₉, were sequentially formed during sintering, we only investigated the crystallization kinetics of the LaBO₃ phase. The kinetic behavior of the LaAl₂B₃O₉ phase will be reported in the next paper.

2.2. Property characterization

2.2.1. Differential thermal analysis (DTA)

The DTA (Thermal analysis 2000 series, DuPont, USA) in NTU and another DTA measurement (Model DTA 910, DuPont Corp., USA) offered by the University of Erlangen-Nurmburg were used to investigate the transformation kinetics of the composites during continuous heat treatment. Glass transition temperatures (T_g) and crystallization peak temperatures (T_p) were determined using a heat rate of 10 °C/min.

2.2.2. Phase quantification

The phase identification and quantification of the sintered composites were investigated by an X-ray diffractometer (XRD, Philips PW1830, Philips Instrument, Netherlands) using Cu K α radiation. The applied voltage and current were 30 kV and 20 mA, respectively. The scan speed was 3°/min and each step was 0.04°. The pure LaBO₃ crystalline phase for quantification XRD analysis was prepared and verified with the following steps: A DTA test of the pure LaBO₃ powder run at 850 °C was carried out. As no thermal effect was recorded until 2 h, and no difference in the X-ray patterns of crystallized standards

was found, a full crystallization in pure LaBO₃ standard was assumed. The patterns of pure LaBO₃ powder and the mixture with calcined Al₂O₃ were used for quantitative analysis. Most of LaBO₃ and α -Al₂O₃ peaks overlap between 30° and 50°, except the indexed peak (1 2 2) of LaBO₃ phase that could be chosen for quantification. The relative amount of crystallized phase presented in the glasses was determined by comparing the major peak intensity ((1 2 2), $2\theta = 44.438^\circ$) of the unknown specimen with those of the standard specimens.

The crystallization kinetics and mechanism have been analyzed in this study according to the Avrami analysis and modified methods. The values of crystallization dimensionality and activation energy of LaBO₃ phase formation were also evaluated.

2.2.3. Microstructural characterization

The sample for SEM observation was ground and lapped with various diamond and Al₂O₃ suspensions. After polishing, the surface was cleaned and dried in a vacuum oven. Thin foils for TEM observation were prepared by typical ion-milling procedures by an ion miller (PIPS, Gatan Co., USA) until a thin, electron-transparent area was obtained. Scanning and transmission electron microscopes (field-emission SEM, Leo Instrument 1530, England; TEM, 100CXII, JEOL Co., Japan and HF-2000 FE-TEM, Hitachi Corp., Japan) were used. Besides, an analytical electron microscope (Tecnai 300 FE-TEM, Philips Instrument Corp., Netherlands) equipped with EDS was used to investigate the elemental distribution in each phase.

3. Results

Previous reports^{1,2} have identified two crystalline phases, LaBO₃ and LaAl₂B₃O₉,^a which may grow in the L2 glass at the temperatures greater than 800 °C. The data of thermal analysis of the L2 glass and two LAB/Al₂O₃ glass–ceramic composites are shown in Fig. 1. The DTA curve of the pure LAB glass shows a distinct endothermic peak (T_g), representing a glass transition, and two exothermic peaks (T_{p1} and T_{p2}), representing the crystallization of the phases, but only one exothermic peak is found in L30A and L40A (L2 glass mixed with 40% Al₂O₃), respectively.

The endothermic glass transition reaction in the DTA curves was due to a change in the heat capacity attributed to the transformation of glass structures. The first exothermic peak depicted the onset crystallization temperature (T_0) and the crystallization peak temperature (T_{p1}) of the LaBO₃ phase. It was noted that pure LAB glass had an additional exothermic peak, which should be the crystallization of the LaAl₂B₃O₉ phase. Besides, the DTA curve of L40A showed T_g , T_0 , and T_p at higher temperatures ($T_g = 760^\circ\text{C}$, $T_0 = 848^\circ\text{C}$, and $T_{p1} = 877^\circ\text{C}$). Most significantly, the second exothermic peak became broad and faded away in the L30A and L40A curves.

^a The phase is indexed as LaAl₂O₃(B₄O₁₀)O_{0.54}, (JCPD file 87-0484), and also indexed by JCPD file 47-1824 as (Ce,La)Al₂B₃O₉. For easy presentation, we use the notation LaAl₂B₃O₉ in the following sections.

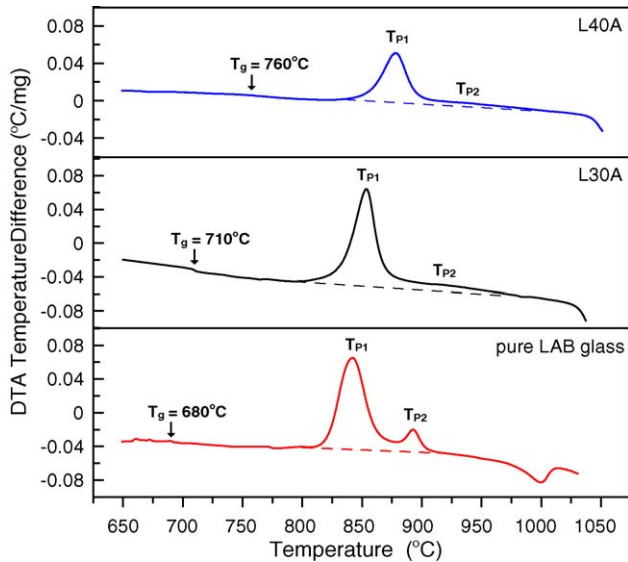


Fig. 1. DTA curves of pure L2 glass, L30A, and L40A glass–ceramic composites at a heating rate of $10^{\circ}\text{C}/\text{min}$. The dotted line was taken as the base line of the curve.

Typical SEM micrographs of the L30A by different sintering conditions are shown in Fig. 2. Homogeneous microstructure without porosity (measured density = $3.57\text{ g}/\text{cm}^3$) was observed in Fig. 2(a), in which the Al_2O_3 particles were in a darker contrast and well distributed in the matrix. The sintering temperature 800°C was able to densify the matrix by a viscous flow of the La–Si–borate glass, but the refractory Al_2O_3 particles did not change apparently.

The morphologies of the polished L30A obtained from second heat-treatment stage ($850^{\circ}\text{C}/1\text{ h}$) were also imaged by a back-scattering electron (BSE) mode, as shown in Fig. 2(b). The Al_2O_3 particles became rounded at the edges (Fig. 2(b)) after treatment at 850°C . This phenomenon implied that Al_2O_3 grain might dissolve into the glassy matrix during the second heat treatment. Therefore, small Al_2O_3 particles or the sharp corners of the Al_2O_3 particles would dissolve. Besides, bulky LaBO_3 crystals grew more in volume when sintering was conducted at temperatures $\geq 800^{\circ}\text{C}$.

The matrix after treatment at 850°C showed additional $\text{LaAl}_2\text{B}_3\text{O}_9$ flaky crystals (in gray contrast) as shown in Fig. 2(b). The flaky crystals with the length longer than $1\text{ }\mu\text{m}$ grew with the orientations in specific pattern and distributed between the granular LaBO_3 and Al_2O_3 phases. The details will be examined by TEM and reported in the following sections.

3.1. Crystallization kinetics of LaBO_3 phase

The LaBO_3 phase was the primary crystalline phase grown in the composite after sintering at $\leq 850^{\circ}\text{C}$. The corresponding bright-field (BF) TEM images and diffraction pattern (DP) of the LaBO_3 phase sintering at 800°C for 30 min in air are shown in Fig. 3. The equiaxial LaBO_3 crystals in the sizes of $0.15\text{--}0.45\text{ }\mu\text{m}$ showed distinct features from the matrix, and mostly surrounded by a glassy layer (Fig. 3(a) and (b)). The glassy layer had a distinct interface with the LaBO_3 grain, imply-

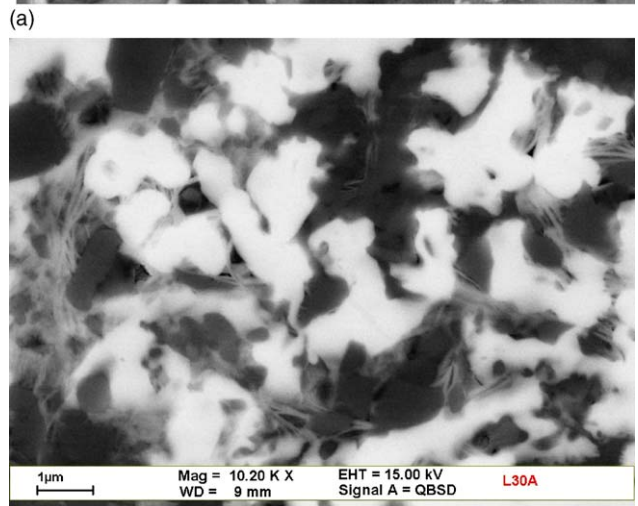
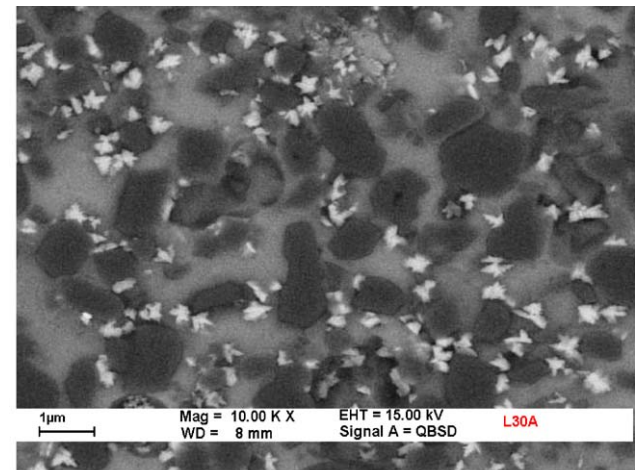


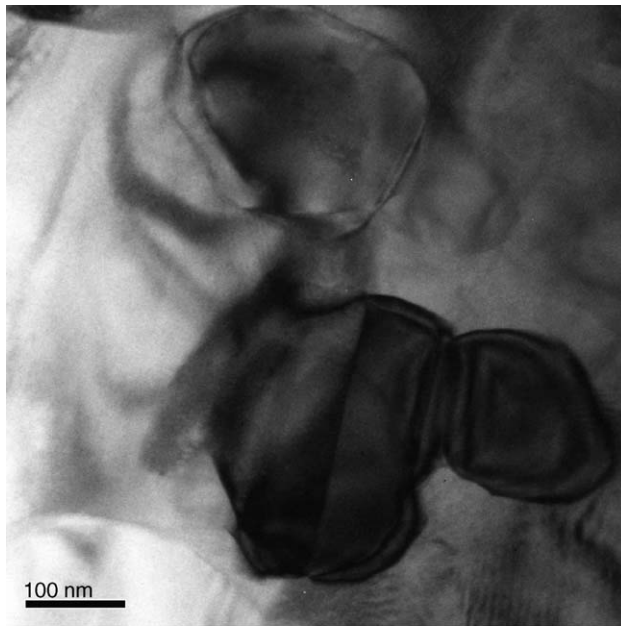
Fig. 2. SEM micrographs by back-scattered electron (BSE) imaging showing the component distribution and crystal phases of L30A sintered at (a) $800^{\circ}\text{C}/1\text{ h}$ and (b) $800^{\circ}\text{C}/1\text{ h}\text{--}850^{\circ}\text{C}/10\text{ min}$ in air at a heating rate of $10^{\circ}\text{C}/\text{min}$.

ing good wetting properties of the borate glass and good thermal expansion matching with the LaBO_3 grain. The high-resolution micrograph (Fig. 3(b)) illustrated the lattice image of (020) plane with $\sim 0.7\text{ nm}$ spacing. As the DP shown in the insert, a broad diffraction ring was resolved, which should be contributed by the amorphous glass in the neighborhood of the LaBO_3 grain.

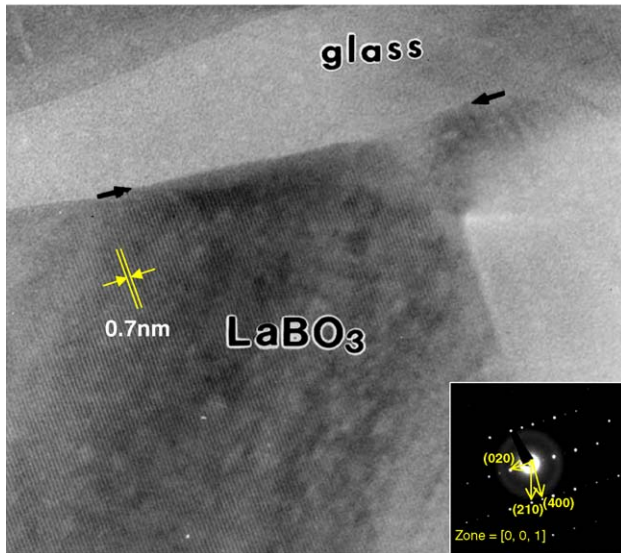
Homogeneous and heterogeneous nucleations of the LaBO_3 phase might occur concurrently at temperatures $\geq 800^{\circ}\text{C}$. It was noted that the formation of LaBO_3 phase started on the glass/ Al_2O_3 interface, evidently judging from the SEM results (Fig. 2(a)). The heterogeneous nucleation is the dominant mechanism during sintering.

A quantification data of the crystalline LaBO_3 phase as a function of the heating rate is shown in Fig. 4. Nearly none of LaBO_3 grew in the matrix at a rate of $25^{\circ}\text{C}/\text{min}$ to $825\text{--}850^{\circ}\text{C}$, but grew to the fraction of $0.8\text{--}0.9$ at a slower rate of $5^{\circ}\text{C}/\text{min}$. In order to consider the effect of quick crystallization, the transformation kinetics was analyzed using the method of continuous heating reported by Kissinger.^{9,10}

Two sets of the DTA tests for either pure L2 glass or L30A glass–ceramic composite are shown in Figs. 5 and 6. The data



(a)



(b)

Fig. 3. TEM images showing the morphologies of L30A by 800 °C/1 h and the LaBO₃ crystals grown from the matrix: (a) two crystals and (b) grain/glass interface and the inserted showing the DP of the LaBO₃ grain.

of the L2 glass showed distinguishable second exothermic peak in the DTA curves compared to those of L30A composite. The DTA results also showed that the crystallization of LAB started to form at a lower temperature than the case in the pure glass, possibly because of the nucleation sites offered by Al₂O₃ filler. The point of heterogeneous nucleation will be discussed in Section 4.1.

The Avrami exponent, n , could be determined from non-isothermal DTA data using the following equation:^{10,11}

$$\frac{d \ln[-\ln(1-x)]}{d \ln \alpha} \Big|_r = -n \quad (1)$$

where x is the volume fraction of a crystallized phase tested at a heating rate of α . As a consequence, the treatments of

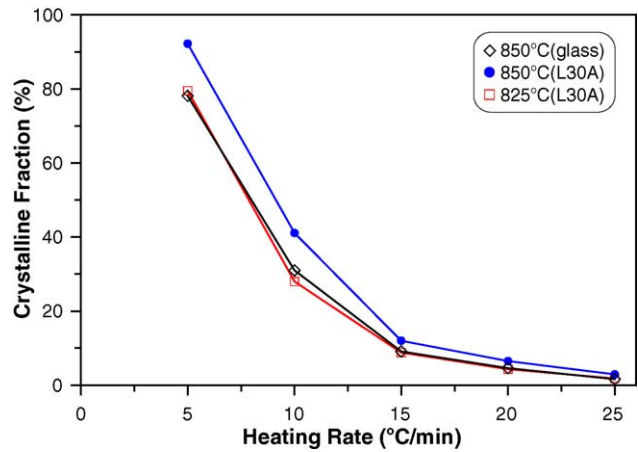


Fig. 4. Amount of LaBO₃ phase growing from L2 glass or L30A glass–ceramic composite at specified temperatures plotted as a function of the heating rate.

$\ln[-\ln(1-x)]$ versus $\ln \alpha$ at various temperatures of pure LAB glass and L30A composite were conducted and the results are shown in Fig. 7. The exponent, n , was determined from the slopes with the values of 2.5–2.7, implying that the crystallization could be one with three-dimensional (3D) growth of LaBO₃ crystals.¹² The analysis data of the crystallization mechanism are similar in pure LAB glass and in L30A composite.

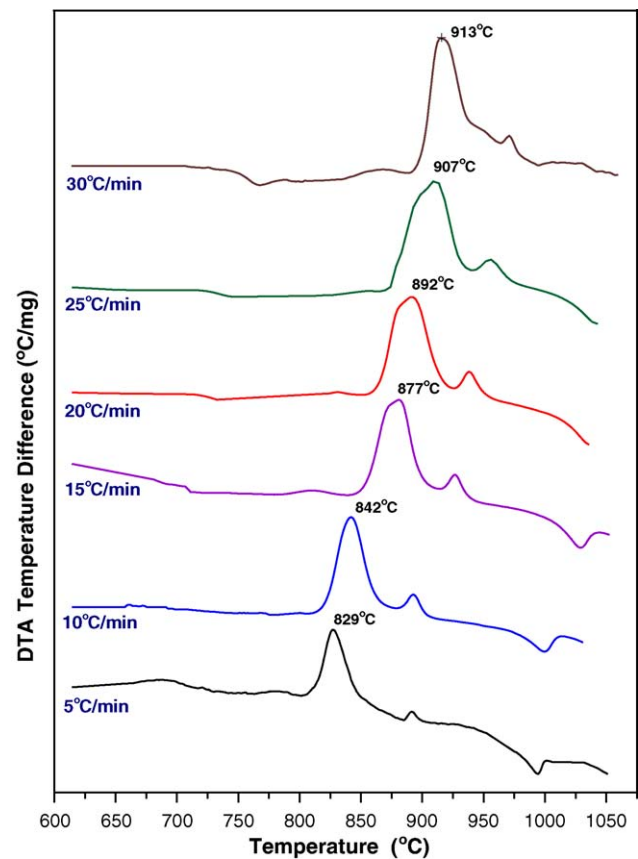


Fig. 5. DTA curves of pure L2 glass testing at different heating rates.

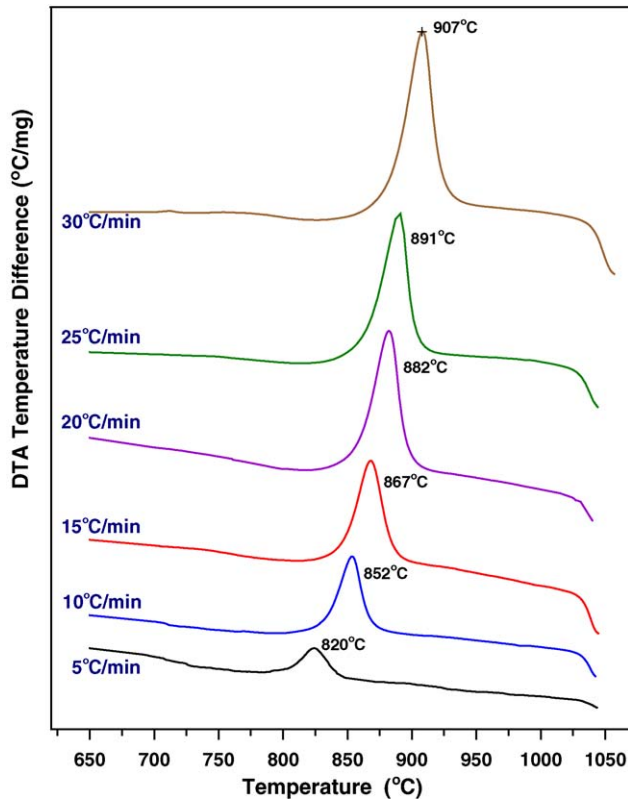


Fig. 6. DTA curves of L30A glass–ceramic composite testing at different heating rates.

The thermal activated process could also be evaluated from the nonisothermal measurements using the following form:¹⁰

$$\ln \frac{\alpha^n}{T_p^2} = \frac{mQ}{RT_p} + \text{const} \quad (2)$$

where m is the dimensionality of the crystal growth and R the gas constant. The value of m equals to n when the crystallization at different heating rates occurs on a constant number of nuclei for nonisothermal mode. In this study, the DTA samples were pre-heated around the nucleation temperature (725 °C) for 1 h, and then underwent various heating-rate treatments. It was assured that the number of nuclei was not dependent on the heating rate for the following two evidences. First, the DTA curves of the pre- and after-heat-treatment had the approximate identical T_0 and T_p points. The second, based on the SEM micrographs, as one typical case shown in Fig. 2(a), the number of LaBO₃ crystals per area were in the range from $4.1 \times 10^6/\text{cm}^2$ to $5.3 \times 10^6/\text{cm}^2$, and remained roughly unchanged with time. This result indicated no formation of new crystals and implied a zero nucleation rate ($\dot{N}=0$) during the heat treatment.

The apparent activation energy, Q , was evaluated from the nonisothermal measurements using this modified Kissinger method. A plot of $\ln(\alpha^n/T_p^2)$ versus $1/T$ is shown in Fig. 8. The best fitting lines of two sets of DTA data were obtained and plotted in the figure. The Q_{L2} (glass) and Q_{L30A} (L30A composite) values calculated from the slopes were 534 ± 15 and 466 ± 15 kJ/mol, respectively. The crystallization processes of pure glass with Al₂O₃ particles appeared at lower acti-

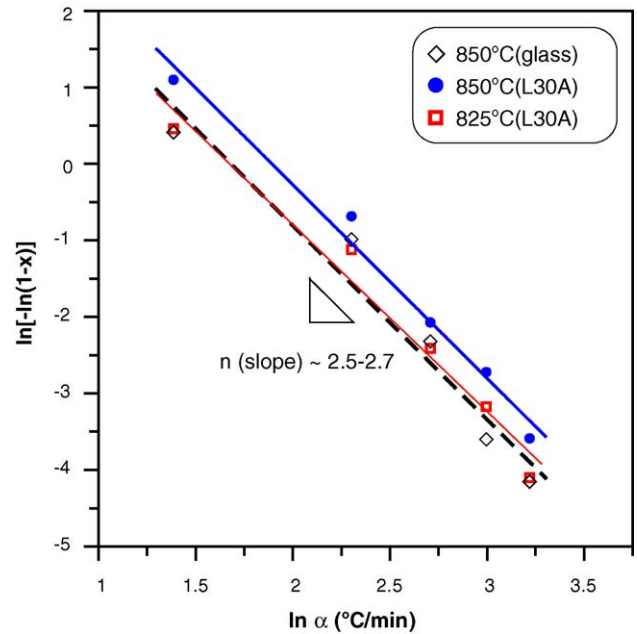


Fig. 7. Analysis results illustrating the amount of phase transformation plotted against the heating rate of pure L2 glass heating at 850 °C, and L30A glass–ceramic composite heating at either 825 or 850 °C.

vation energy ($\Delta Q \simeq 60$ kJ/mol) than that of the pure glass (L2).

3.2. Formation of LaAl₂B₃O₉

In addition to LaBaO₃ phase, LaAl₂B₃O₉ phase was identified in the matrix (Fig. 2(b) and Fig. 9). As the TEM micrograph appeared, four regions (A, B, C, and D) were examined by electron diffraction, revealing regions A and C to be α -Al₂O₃, region B to be LaBO₃ phase, and region D (flaky features) to be

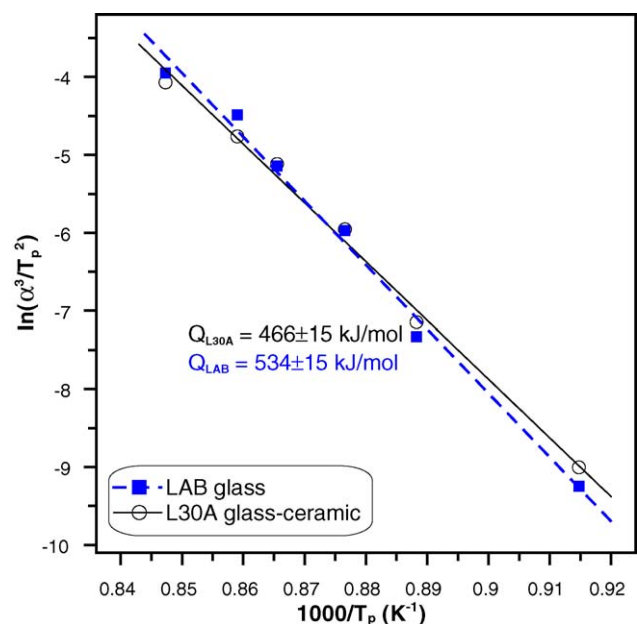


Fig. 8. Analysis results of pure LAB glass (Q_{LAB}) and L30A glass–ceramic composite (Q_{L30A}) testing at different temperatures.

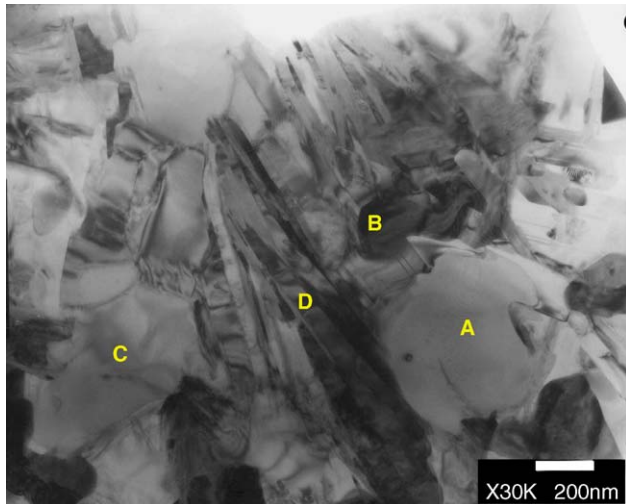


Fig. 9. TEM bright field (BF) image showing the grain morphologies and phase distribution of L30A glass–ceramic composite sintered at 800 °C/1 h, then 850 °C/10 min in air at a heating rate of 10 °C/min. The grains of A (and C), B, and D were identified as Al_2O_3 , LaBO_3 , and $\text{LaAl}_2\text{B}_3\text{O}_9$ phases, respectively (see Section 3.2).

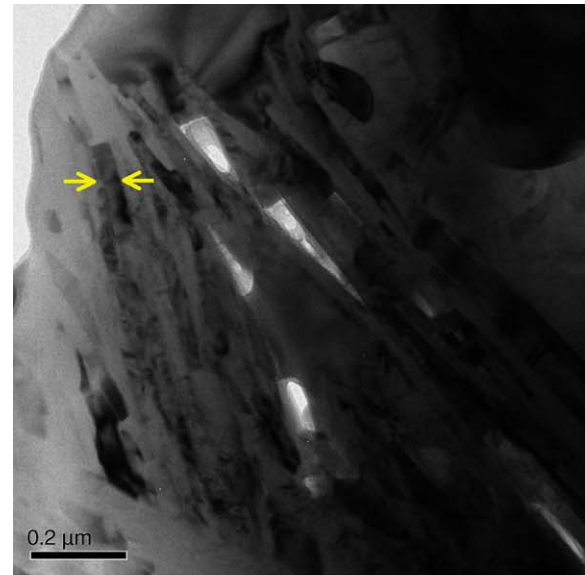
$\text{LaAl}_2\text{B}_3\text{O}_9$ phase. The Al_2O_3 grains were equiaxial and exhibited a size distribution of submicrometer. Besides, Al_2O_3 grains showed very few defects, such as dislocation or faults included in the grains after sintering.

Flaky $\text{LaAl}_2\text{B}_3\text{O}_9$ crystals were studied and revealed in Figs. 10–12. The TEM images showed that the anisotropic flaky crystals were mostly formed after annealing at ≥ 850 °C. The crystals showed a high aspect ratio with a thickness of ca. 50 nm. Centered dark-field (CDF) imaging shown in Fig. 10(b) illustrated that the crystals might have a similar orientation by a diffraction intensity of (002), as shown in the selected-area DP in Fig. 10(c). The bright regions in the CDF micrograph also showed that the crystalline orientation between the neighboring $\text{LaAl}_2\text{B}_3\text{O}_9$ crystals were close, implying that the growth of those flaky crystals came from the same nucleus.

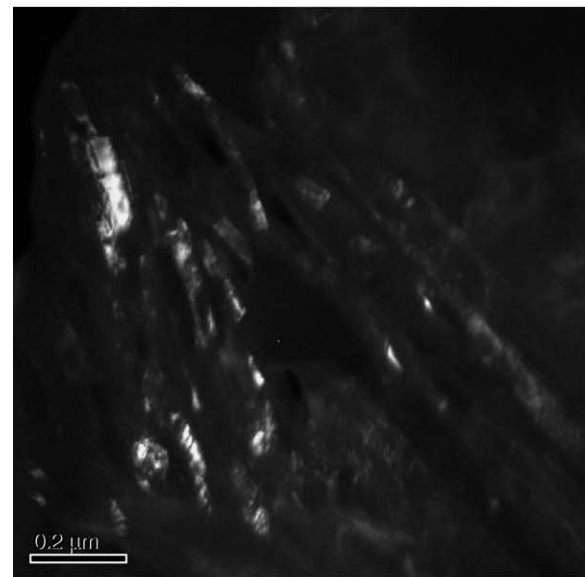
When the L30A sample was heat-treated at 950 °C, which was 100 °C greater than the normal conditions used in the previous data (Fig. 10), a series of SEM and TEM micrographs of the L30A composite were taken. The images showed that the flaky $\text{LaAl}_2\text{B}_3\text{O}_9$ crystals had grown to the lengths of several micrometers (Fig. 11(b)), but LaBO_3 grains were hardly found in the matrix. The LaBO_3 grains must have reacted with the neighboring species to form flaky grains.

The results of a shrinkage test of the L30A composite were reported in Fig. 11(c), of which the rate decreased at ≥ 810 °C and turned to expand at temperatures > 880 °C. The change in the shrinkage rate is due to the crystal growth of $\text{LaAl}_2\text{B}_3\text{O}_9$. The formation of $\text{LaAl}_2\text{B}_3\text{O}_9$ crystals was contributed by a reaction of LaBO_3 with Al_2O_3 filler and/or glassy matrix. The reaction took place at the temperatures ≥ 810 °C, and became more evident above 880 °C.

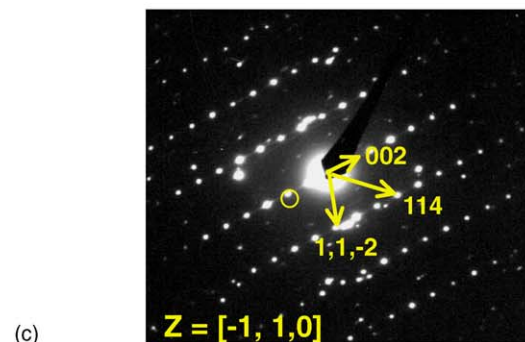
Detailed interfacial investigation of $\text{Al}_2\text{O}_3/\text{LaAl}_2\text{B}_3\text{O}_9/\text{Al}_2\text{O}_3$ was conducted and shown in Fig. 12. According to the compositional analysis, the Al and La elemental line scanning in Fig. 12(b) revealed a diffusion layer of about 30 nm, showing a



(a)



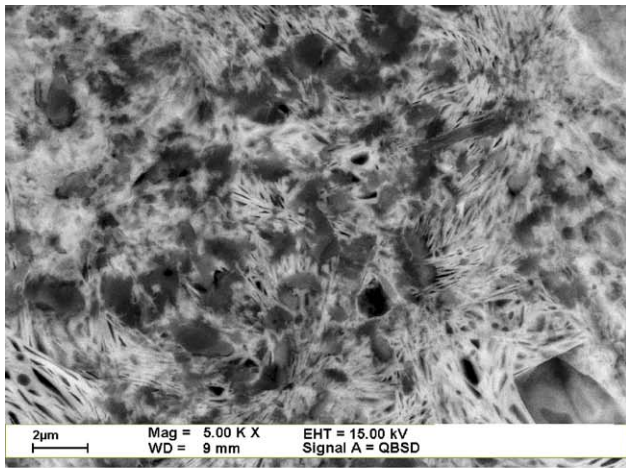
(b)



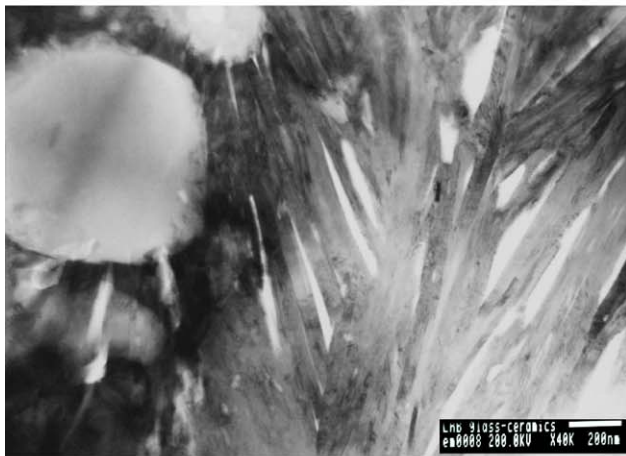
(c)

Fig. 10. TEM morphologies of $\text{LaAl}_2\text{B}_3\text{O}_9$ crystals grown in L30A sintered at 800 °C/1 h–850 °C/10 min. (a) BF; (b) CDF; (c) with the corresponding DP and zone pattern of $[-1, 1, 0]$.

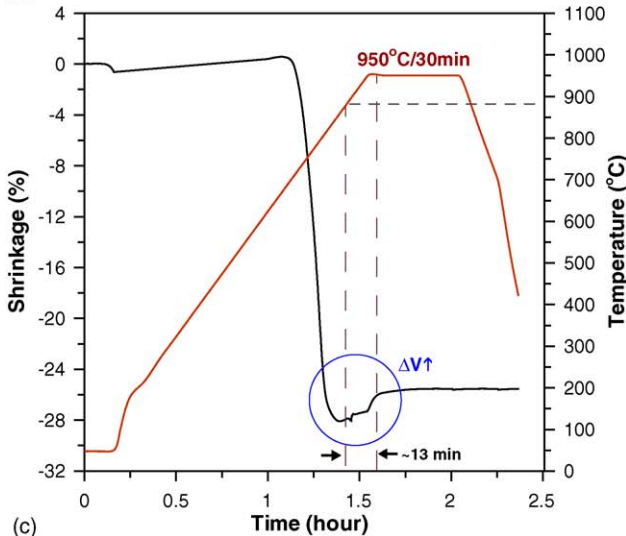
gradient Al_2O_3 content between $\text{LaAl}_2\text{B}_3\text{O}_9/\text{Al}_2\text{O}_3$ interfaces. The $\text{LaAl}_2\text{B}_3\text{O}_9$ phase was predominantly nucleated on the Al_2O_3 surface. Furthermore, the amorphous phase was always found at the grain triple junction between $\text{LaAl}_2\text{B}_3\text{O}_9$ and Al_2O_3



(a)



(b)

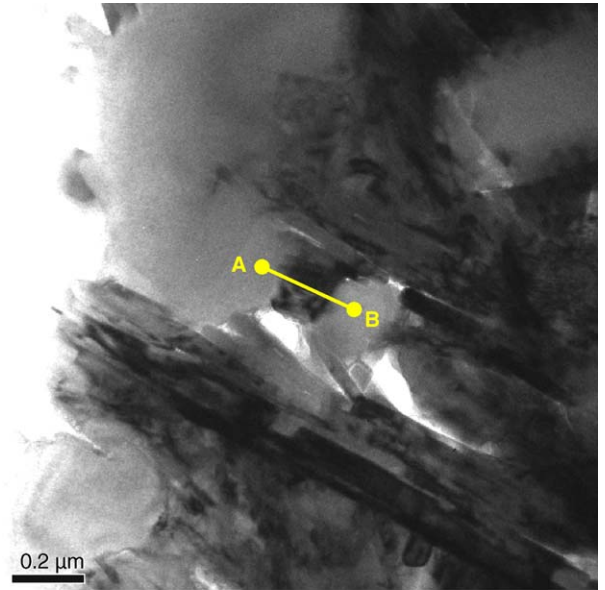


(c)

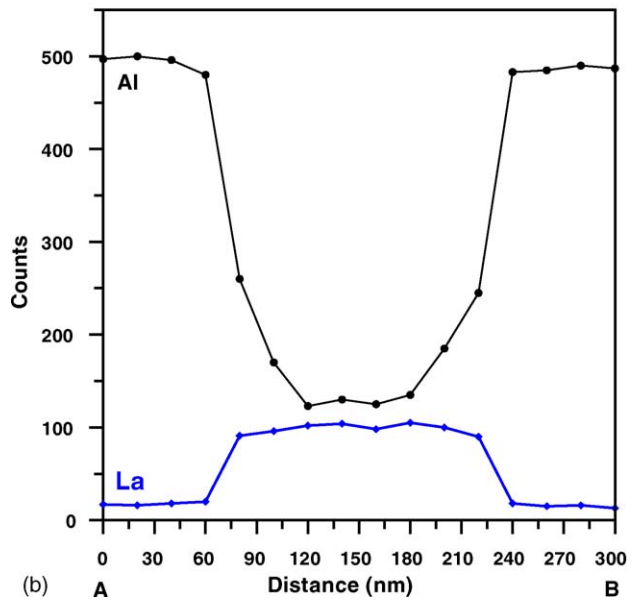
Fig. 11. (a) SEM, (b) TEM micrographs showing the flaky crystals of L30A, and (c) dilatometric curve showing an obvious volume expansion starting at 880 °C.

grains (Fig. 13). These glass phases could offer the diffusion path for the formation of $\text{LaAl}_2\text{B}_3\text{O}_9$.

The interface between $\text{Al}_2\text{O}_3/\text{LaAl}_2\text{B}_3\text{O}_9$ is continuous. The $d_{(112)}$ of $\text{LaAl}_2\text{B}_3\text{O}_9$ crystal is 2.068 nm, which is close to $d_{(006)}$ of $\alpha\text{-Al}_2\text{O}_3$ phase, 2.165 nm. The difference of the lattice space between $\text{LaAl}_2\text{B}_3\text{O}_9/\text{Al}_2\text{O}_3$ is $\leq 5\%$. The interface misfits for



(a)



(b)

Fig. 12. (a) TEM micrograph of L30A sintering at 800 °C/1 h–850 °C/10 min and (b) qualitative compositional profiles of Al and La elements near the $\text{Al}_2\text{O}_3/\text{LaAl}_2\text{B}_3\text{O}_9/\text{Al}_2\text{O}_3$ interface.

one (1 1 2) lattice plane every 25–26 layers, implying that the interface of $\text{LaAl}_2\text{B}_3\text{O}_9/\text{Al}_2\text{O}_3$ (Fig. 13)) is still semicoherent. Also, as the matching layers become more than 26 (ca. 50 nm), one new $\text{LaAl}_2\text{B}_3\text{O}_9$ nucleus grows at the triple junction of $\text{Al}_2\text{O}_3/\text{LaAl}_2\text{B}_3\text{O}_9/\text{glass}$. As a result (Figs. 10–13), the crystals of $\text{LaAl}_2\text{B}_3\text{O}_9$ showed a platy feature in two-dimensional radial extension from Al_2O_3 surfaces.

4. Discussion

4.1. Heterogeneous nucleation of LaBO_3

In order to assure the heterogeneous nucleation of LaBO_3 phase, which is induced at the interface of $\text{Al}_2\text{O}_3/\text{L2}$ glass, one

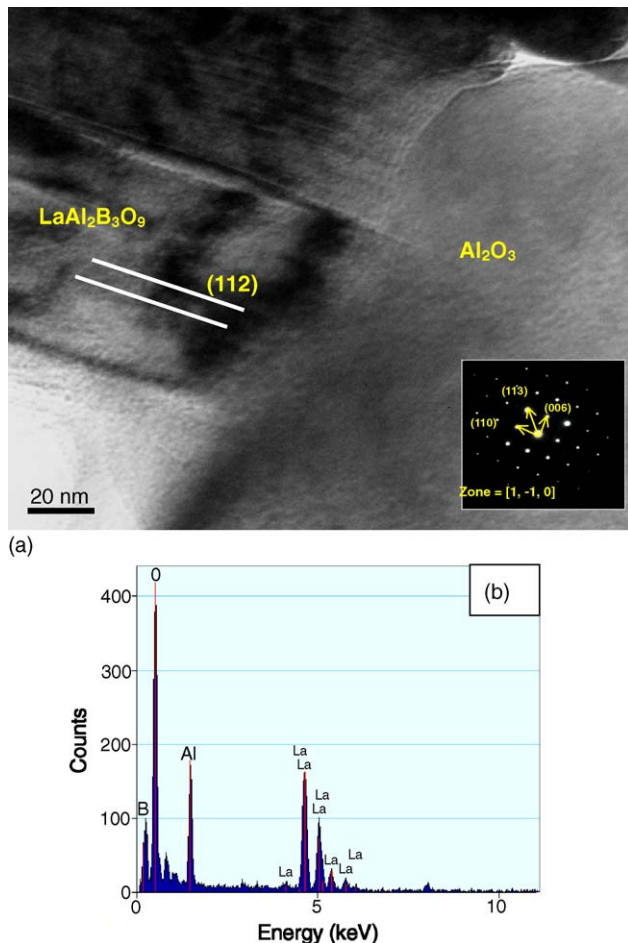


Fig. 13. (a) TEM image of $\text{LaAl}_2\text{B}_3\text{O}_9/\text{Al}_2\text{O}_3$ grains with the inserts of one DP illustrating the crystalline orientation of the Al_2O_3 and (b) EDS spectrum of a glass composition.

sample consisting of 70% L2 glass and 30% ultra-fine $\alpha\text{-Al}_2\text{O}_3$ powder (AKP-50, 0.3 μm average size, surface area 5.02 m^2/gm) was prepared. After sintering at 800 $^\circ\text{C}$ for 1 h, the same sintering condition as L30A (Fig. 2(a)), the polished surface (Fig. 14) showed significant difference in the nucleation density of LaBO_3 crystals in the sample. More LaBO_3 crystals (a higher crystalline density) could be found on the $\text{Al}_2\text{O}_3/\text{glass}$ interface. Crystalline clusters in the matrix were also observed. The number density of LaBO_3 crystals was $1.7 \times 10^7/\text{cm}^2$, which was about two times higher than the density shown in Fig. 2. The finer Al_2O_3 filler offered more nucleation sites due to a higher specific surface area of Al_2O_3 used for L30A.

The formation of LaBO_3 in L2 glass has an activation energy of $534 \pm 15 \text{ kJ/mol}$, which is higher than that in L30A, because most of the nucleation takes place on the heterogeneous sites. The difference in the activation energy of Q_{LAB} and Q_{L30A} is about 68 kJ/mol , which implies that the formation of LaBO_3 crystals on the $\text{Al}_2\text{O}_3/\text{glass}$ interfaces in the L30A is easier than the growth in pure L2 glass. The difference in the activation energy between LAB glass and L30A glass–ceramic composite is mainly due to heterogeneous nucleation. The site density for nucleation is proportional to the available $\text{Al}_2\text{O}_3/\text{glass}$ interface area.

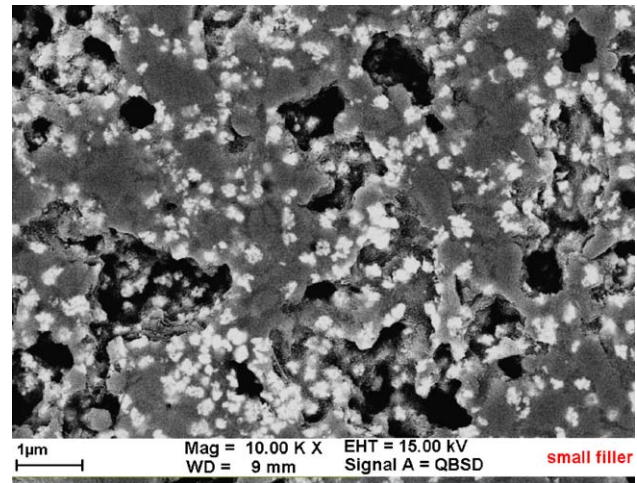


Fig. 14. SEM micrographs in showing the equiaxial LaBO_3 crystals in a L30A formulation with fine $\alpha\text{-Al}_2\text{O}_3$ filler (average size 0.3 μm) sintered at 800 $^\circ\text{C}$ for 1 h in air at a heating rate of 10 $^\circ\text{C}/\text{min}$.

4.2. Transformation kinetics of LaBO_3

It has been shown by Ozawa that the validity of Eq. (2) could be extended under certain circumstances for nonisothermal conditions. Two simple models for the case of crystal growth from pre-existing nuclei were proposed.¹³ One is the crystal growth from impurity or nucleation agent, where the number of nuclei is independent upon the thermal history of the material. The second model was about the case of random (homogeneous) nucleation clearly separating from its following crystal growth. So the number of the nuclei was changing during the crystal growth. The L30A glass–ceramic system in this study, therefore, belongs to the first model.

In this study, Avrami exponent n (Fig. 7) was measured, and was nearly independent of the heating rate. Possible values of n for different crystallization mechanisms are 1–4. If the values of m and n are equal for the cases, 3D crystallization is the predominant mechanism. The shape of LaBO_3 grains shown in Figs. 2 and 3 supported the evidences of 3D growth of the crystals in the L30A sample. Besides, the nucleation mechanism is the interface control as n equals to 3.⁸

4.3. Effect of Al_2O_3 on phase evolution

Previous analysis showed that L2 glass had no apparent reaction with Al_2O_3 filler below (710 $^\circ\text{C}$). The L2 glass did not form a liquid phase until the temperature reached T_g (710 $^\circ\text{C}$). Due to the softening of the L2 glass, the glass penetrated into the space between Al_2O_3 particles, leading to some degrees of dimensional shrinkage and grain dissolution. However, the composite still contained some visible pores and grew LaBO_3 grains at the glass/ Al_2O_3 interface. At the temperatures higher than T_0 (820 $^\circ\text{C}$), the sintering rate of the LAB glass decreased, in the meantime, the LaBO_3 crystals started to react with Al_2O_3 particles at the interfaces to form flaky $\text{LaAl}_2\text{B}_3\text{O}_9$, and showed a fairly fast growing rate when treated at 900 $^\circ\text{C}$. The final microstructure of L30A composite consisted of residual Al_2O_3

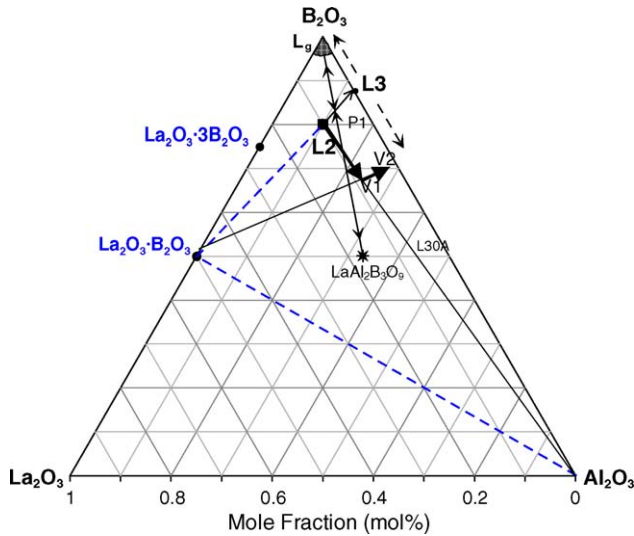
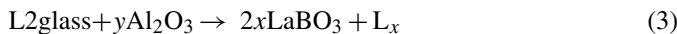


Fig. 15. Crystallization paths of LaBO_3 and $\text{LaAl}_2\text{B}_3\text{O}_9$ phases in the ternary La–Al–B–O system.

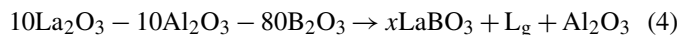
grains, newly grown $\text{LaAl}_2\text{B}_3\text{O}_9$ plate grains, and La–Al–B–O glass.

The diffusion of Al^{3+} species by the dissolution of Al_2O_3 filler is the dominating factor for the reactions at temperatures above 710°C . The reaction involves three possible stages. The first stage is the dissolution of Al_2O_3 between 710 and 800°C , of which the glass in a composition $10\text{La}_2\text{O}_3\text{--}10\text{Al}_2\text{O}_3\text{--}80\text{B}_2\text{O}_3$ (L2) increases Al–O content as shown by the V_1 trajectory. In addition, the process will simultaneously trigger the formation of LaBO_3 (V_2 trajectory). Therefore, the combination of Al_2O_3 dissolution and the crystallization reaction of LaBO_3 can be shown as below.



The composition of the L2 glass moves along the V_3 ($V_1 + V_2$) trajectory as the composition of L_x ($10 - x$) $\text{La}_2\text{O}_3 - (10 + y)$ $\text{Al}_2\text{O}_3 - (80 - x)$ B_2O_3 . The LaBO_3 grains formed finely divided crystalline phase next to the glass and Al_2O_3 grains.

The second possibility of the formation of LaBO_3 phase is that the glass readily decomposes (a peritectic reaction) in accompany with the formation of L_g and Al_2O_3 .



where L_g glass is a B_2O_3 -rich (>95%) glass. The reaction is similar to the crystallization along the boundary of two primary fields. But no evidence of new Al_2O_3 grains was found. Therefore, the reaction of Eq. (3) is more likely dominating in the system.

The third stage of the reaction is the formation of $\text{LaAl}_2\text{B}_3\text{O}_9$ phase, which could be triggered as LaBO_3 phase is formed. Two possible reaction routes are considered. One is a ternary peritectoid reaction, as the reaction of P1 shown in Fig. 15.



The other possible reaction involves the reaction of LaBO_3 and Al_2O_3 , shown as below:



where L_p is the peritectic liquid induced in the ternary diagram. The evidence showed that the volume fraction of Al_2O_3 grains decreased (Figs. 2(b) and 11(a)) through only 10 mol% Al_2O_3 in the glass formulation, but 44 vol%^b in the L30A. Therefore, the DTA curve (Fig. 1) showed that second exothermic crystallization peak (T_{P2}) faded away and broadened, implying the $\text{LaAl}_2\text{B}_3\text{O}_9$ phase was able to form at lower temperatures owing to the availability of Al_2O_3 ingredient.

Nanobeam EDS analysis obtained without the boron window presented the composition of the glass phase, which consisted of La, Al, B, and O elements. The $\text{LaAl}_2\text{B}_3\text{O}_9$ is thermodynamically stable and coexists with Al_2O_3 and La–Al–B–O glass but not with B–O glass (L_g). Therefore, the EDS result supports that the phase formation of $\text{LaAl}_2\text{B}_3\text{O}_9$ is possibly following Eq. (6).

5. Conclusion

Two crystalline phases, LaBO_3 and $\text{LaAl}_2\text{B}_3\text{O}_9$, dominantly grow in $\text{La}_2\text{O}_3\text{--Al}_2\text{O}_3\text{--B}_2\text{O}_3$ glass–ceramic composites at temperatures above 710°C by nucleation and growth mechanism. LaBO_3 crystals growing in equiaxial shape undergo the heterogeneous nucleation at specific sites on Al_2O_3 grain surface. The crystallization activation energy of LaBO_3 phase in pure L2 glass and L30A glass–ceramic composite were evaluated as 534 ± 15 and 466 ± 15 kJ/mol, respectively. The difference in the activation energy (68 kJ/mol) was due to the heterogeneous nucleation on Al_2O_3 grain surface. Besides, the number density of LaBO_3 crystals remained constant with the heating time, indicating a zero nucleation rate in the process. The analysis on the microstructural evolution reported the values of Avrami constant (n) in the range of 2.5 to 2.7, confirming that the formation of the LaBO_3 crystal was a three-dimensional bulk crystallization. The microstructural observations by SEM/TEM were in agreement with the data by kinetics analysis.

$\text{LaAl}_2\text{B}_3\text{O}_9$ flaky grew at temperatures $\geq 850^\circ\text{C}$. The crystals were generated after the formation of LaBO_3 phase and grew from the triple junction of the LaBO_3 , Al_2O_3 , and glass phase. The crystal growth of $\text{LaAl}_2\text{B}_3\text{O}_9$ showed similar platy features in radial directions from the Al_2O_3 surfaces by the reaction of La–Al–B–O glass/ Al_2O_3 / LaBO_3 .

Acknowledgments

The authors like to thank Institute of Glass and Ceramics at University of Erlangen-Nuremberg, Germany, for kindly providing laboratory facility, and the financial supported by PPP (0910044476) in Germany and NSC (92-2911-I-002-011) in Taiwan.

^b Due to the presence of glassy phase, we are not able to estimate the density and molecular weight of the phase. Therefore, a rough estimation of alumina molar content in L30A is reported.

References

1. Wei, W. C. J., Chen, C. L. and Roosen, A., La₂O₃/Al₂O₃/B₂O₃ based glass–ceramics for LTCC application. *Key Eng. Mater.*, 2005.
2. Chen, C. L., Wei, W. C. J. and Roosen, A., Wetting, densification and phase transformation of La₂O₃/Al₂O₃/B₂O₃ based glass–ceramics. *J. Eur. Ceram. Soc.*, in press.
3. 943 tape, DuPont.
4. Shelleman, R. A., Messing, G. L. and Kumagai, M., Alpha-alumina transformation in seeded boehmite gels. *J. Non-Cryst. Solids*, 1986, **82**, 277–285.
5. Kao, H. C. and Wei, W. J., Kinetics and microstructural evolution of heterogeneous transformation of θ -alumina to α -alumina. *J. Am. Ceram. Soc.*, 2000, **83**(2), 362–368.
6. Yu, B., Liang, K. and Gu, S., Effect of ZrO₂ on crystallization of CaO–P₂O₅–SiO₂ glasses. *Ceram. Int.*, 2002, 695–698 (28).
7. Marrota, A., Buri, A., Branda, F. and Saiello, S., Nucleation and crystallization of LiO₂–2SiO₂ glass—a DTA study. In *Advances in Ceramics, Nucleation and Crystallization in Glasses, Vol 4*, ed. J. H. Simmons, D. R. Uhlmann and G. H. Beall. American Ceramic Society, Columbus, OH, 1982, pp. 146–152.
8. Brown, W. E., Dollimore, D. and Galwey, A. K., Comprehensive chemical kinetics. In *Reactions in the Solid State, Vol 22, Chap. 3*, ed. C. H. Bamford and C. F. H. Tipper. Elsevier, Oxford, UK; New York, 1980.
9. Kissinger, E., Reaction kinetics in differential thermal analysis. *Anal. Chem.*, 1957, **29**(11), 1702–1706.
10. Matusita, K. and Sakka, S., Kinetic study on crystallization of glass by differential thermal analysis criterion on application of Kissinger plot. *J. Non-Cryst. Solids*, 1980, **741–746**, 38–39.
11. Yinnon, H. and Uhlmann, D. R., Application of thermo-analytical techniques to the study of crystallization kinetics in glass-forming liquids. Part I: theory. *J. Non-Cryst. Solids*, 1983, **54**, 253–275.
12. Henderson, D. W., Experimental analysis of nonisothermal transformation involving nucleation and growth. *J. Therm. Anal.*, 1979, **15**(2), 325–331.
13. Ozawa, T., Nonisothermal kinetics of crystal growth from pre-existing nuclei. *Bull. Chem. Soc. Jpn.*, 1984, **57**, 639–643.